ELSEVIER

Journal of Alloys and Compounds 323–324 (2001) 605–609

Journal of ALLOYS AND COMPOUNDS

www.elsevier.com/locate/jallcom

Surface properties of $CeZrO_4$-based materials employed as catalysts supports

A. Martínez-Arias*, M. Fernández-García, A.B. Hungría, J.C. Conesa, J. Soria

Instituto de Catálisis, CSIC, Campus UAM, Cantoblanco, 28049 Madrid, Spain

Abstract

The surface properties of high surface area $CeZrO_4$, 10 wt.% $CeZrO_4/\gamma$-Al_2O_3 and 33 wt.% $CeZrO_4/\gamma$-Al_2O_3 samples, prepared by a reverse microemulsion synthesis method, have been studied by FTIR and EPR, employing, respectively, CH_3OH and O_2 as probe molecules. Observation of on-top methoxy species adsorbed both on Zr^{4+} and Ce^{4+} (C–O stretching bands appearing at, respectively, ca. 1156 and 1104 cm^{-1}) upon methanol adsorption on the outgassed samples and the red shift of the former with respect to pure zirconia or ZrO_2/Al_2O_3 evidences the presence of a mixed oxide type structure at the surface of the samples. EPR analysis of O_2^- species generated upon O_2 adsorption on the outgassed samples reveals the presence of both dispersed (2D) and aggregated (3D) mixed oxide entities in Al_2O_3-supported samples. Redox differences between these entities have been revealed, 2D entities showing a higher reducibility while they are more difficult to be oxidised. Differences in the surface redox and structural properties of 3D particles on alumina with respect to unsupported $CeZrO_4$ are attributed to an epitaxial relationship between the small size (ca. 2–3 nm) 3D mixed oxide particles and the alumina surface.

Keywords: TWC; Zirconia–ceria mixed oxide; Alumina; Methoxy FTIR; Superoxide EPR

1. Introduction

At present, CeO_2–ZrO_2 mixed oxides containing three-way catalysts (TWCs) constitute the most advanced technology for elimination of pollutants in automobile exhausts [1]. The ceria–zirconia component enhances the behaviour of the classically employed ceria promoter due to its higher oxygen storage capacity (OSC) and resistance to thermal aging, the best compromise between both beneficial effects being reached for Ce:Zr atomic ratios close to unity [2]. The redox properties, including OSC, of Ce–Zr materials are dependent on the geometrical structure of the mixed oxide [3]. So, optimum performance under reaction conditions would correspond to mixed oxides of composition $Ce_xZr_{1-x}O_2$ (with x close to 0.5) which show a pseudo-cubic t'' phase, i.e. displaying an X-ray diffraction pattern indexable in the cubic *Fm3m* space group but having internally tetragonal symmetry ($P4_2/nmc$) due to oxygen displacement from ideal fluorite sites [4,5]. It must be noted that, as a bulk material, the t'' phase is not thermodynamically stable at room temperature (RT) for a 1:1 Ce:Zr atomic ratio, but is supposed to be stabilized for small crystallite sizes [3].

In addition to bulk properties, it is important to obtain a deeper knowledge on the surface properties of these materials as their catalytic behaviour, particularly at low temperature, strongly depends on those properties. For that purpose, in the present work, high surface area materials prepared by a method based on precipitation of the components within reverse microemulsions [6] are examined by FTIR and EPR techniques, using, respectively, methanol and oxygen as probe molecules. As shown in previous works [7–9], analysis of the C–O stretching mode of methoxy species generated upon methanol adsorption can yield information on the kind of exposed surface cations as well as on surface morphological modifications with respect to reference single oxides. On the other hand, EPR analysis of the superoxide species generated upon oxygen adsorption on the reduced samples can give important information at both structural and redox levels about surface properties of these materials [10].

2. Experimental

The $CeZrO_4$ sample was prepared by coprecipitation within a reverse microemulsion, as described in detail

*Corresponding author. Fax: +34-91-585-4760.

E-mail address: amartinez@icp.csic.es (A. Martínez-Arias).

0925-8388/01/$ – see front matter
PII: S0925-8388(01)01189-6

elsewhere [6]. Zirconyl nitrate and cerium (III) nitrate hexahydrate were used as precursor salts and tetramethylammonium hydroxide pentahydrate as base. The precipitated solid was dried for 24 h at 383 K and finally calcined in air for 2 h at 773 K (using a ramp of 2 K min^{-1}). This sample (referred to as CZ) showed S_{BET}=96 m^2g^{-1}. The same method was applied for preparing two ceria–zirconia/alumina samples with 10 and 33 wt.% content of $CeZrO_4$ (10CZA and 33CZA; S_{BET}=186 m^2g^{-1} and S_{BET}=164 m^2g^{-1}, respectively), as described in detail elsewhere [11], and a reference 6 wt.% ZrO_2/Al_2O_3 sample. For these cases, appropriate amounts of γ-Al_2O_3 powder (Condea Puralox, S_{BET}=180 m^2g^{-1}) were incorporated to the reverse emulsion containing the aqueous solution of the precursor nitrates prior to precipitation upon addition of the base microemulsion. Chemical analysis by ICP-AES confirmed full precipitation of Zr and/or Ce components in the samples.

Infrared spectra were recorded at RT with a Nicolet 5ZDX FTIR spectrometer. Self-supporting discs of the samples (containing 10–15 mg cm^{-2}) were prepared and handled with a conventional static IR cell. Methanol adsorption was performed at RT on samples pretreated under O_2 (300 Torr) at 773 K followed by outgassing at 773 K. Following methanol adsorption, the samples were outgassed at 373 K.

Electron paramagnetic resonance (EPR) spectra were recorded at 77 K with a Bruker ER 200 D spectrometer operating in the X-band and calibrated with a DPPH standard (g=2.0036). Portions of ca. 30 mg were placed inside a quartz probe cell using a conventional dynamic high-vacuum line for outgassing or adsorption experiments. Oxygen (210 μmol g^{-1}) adsorption was carried out at 77 K, followed by 30 min warming to RT and overnight outgassing at 77 K (this treatment will be referred to as oxygen adsorption at RT).

3. Results and discussion

3.1. Bulk structural properties of the Ce–Zr mixed oxide

Previous works have studied in detail, by XRD, TEM-EDX and Raman, the morphological bulk properties of the samples studied in the present work [6,11]. For the sake of a better understanding of the results described below, concerning surface properties, a brief summary of the conclusions reached in those works is given at this point. Regular crystallites, displaying a narrow size distribution (ca. 5 nm particles) and presenting the mixed oxide t'' (pseudocubic) phase structure corresponding to a composition close to the nominal Ce/Zr=1, were observed for the CZ sample.

On the other hand, 10CZA and 33CZA displayed [11] a high dispersion of the Ce–Zr mixed oxide, presenting particles with an average size around 2–3 nm, which increases weakly with the CZ loading. The mixed oxide structure t'' was observed in both cases, the 10CZA sample showing a reasonably homogeneous composition with a Ce/Zr ratio close to 1, while the corresponding mixed oxide in 33CZA presented a more heterogeneous nature showing a crystalline phase which on average, and according to the XRD data, can be described as $Ce_{0.60}Zr_{0.40}O_4$; this suggests that a part of the Zr is not detected by any of the diffraction techniques and must be in a nearly amorphous form, as also occurs in CeO_2–ZrO_2/Al_2O_3 specimens prepared by co-impregnation [12].

3.2. Surface structural and redox properties of the Ce–Zr mixed oxide

Previous works have shown the power of using methanol as probe molecule for surface characterisation of Ce–Zr mixed oxide based materials [7–9]. Methanol adsorption is dissociative over this kind of material, giving rise to formation of adsorbed methoxy groups [7]. In the case of pure zirconia, the C–O stretching band of those species appears at 1163 cm^{-1} and 1070 cm^{-1}, corresponding to, respectively, on-top and doubly bridging species adsorbed on zirconium cations [7]. Similar bands appear for pure ceria at 1107, 1063–1042 and 1014 (weak) cm^{-1}, corresponding, respectively to on-top, doubly bridging and triply bridging methoxy species adsorbed on cerium cations [7]. For Ce–Zr mixed oxide samples, both the intensity and frequency of non-overlapping bands of on-top species have been employed to extract information on the surface composition and structure of the samples [7,9]. Fig. 1a–c show the IR spectra in the C–O stretching region of methoxy species formed on CZ, 33CZA and 10CZA

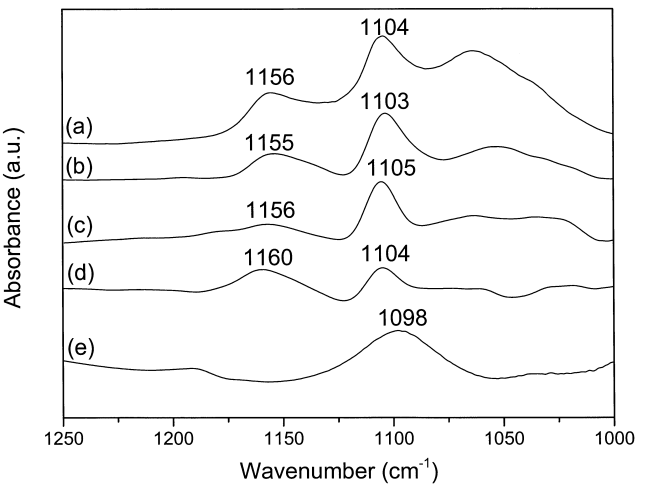

Fig. 1. FTIR spectra in the C–O stretching region formed upon methanol adsorption at RT on the samples outgassed at 773 K, followed by outgassing at 373 K. (a) CZ; (b) 33CZA; (c) 10CZA; (d) ZrO_2/Al_2O_3; (e) Al_2O_3. Spectra (b–d) were obtained after subtracting the alumina reference spectrum (e).

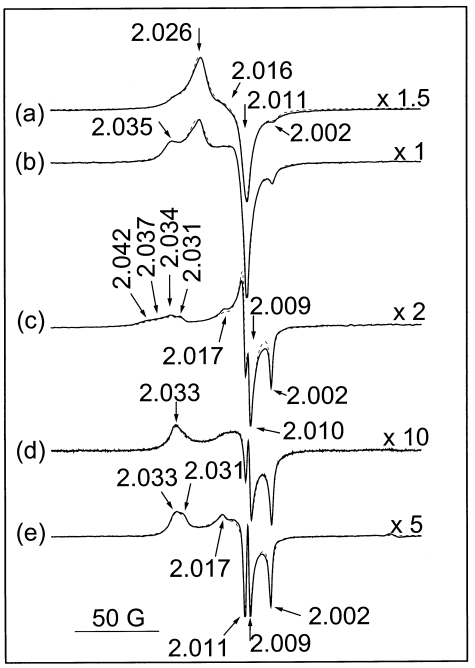

Fig. 2. EPR spectra at 77 K following oxygen adsorption at RT on the samples outgassed at 773 K. (a) 10CZA; (b) 33CZA; (c) CZ. Subsequent outgassing at RT of (d) 10CZA; and (e) 33CZA. Computer simulations are overlapped as dashed lines.

samples. In the three cases, there appear bands of on-top methoxy adsorbed on zirconium and cerium cations at, respectively, ca. 1156 and 1104 cm^{-1}. The presence of both bands reflects that both types of cations are exposed at the surface of the samples. On the other hand, the red shift of the band of on-top methoxy species adsorbed on zirconium cations with respect to that observed on pure zirconia or on the Al_2O_3-dispersed zirconia reference (Fig. 1d) is characteristic of the presence of a mixed oxide structure at the surface of the samples [7,9]. It must be noted that the presence of a broad methoxy band centred at 1098 cm^{-1} for the alumina reference (Fig. 1e) and of a band at 1104 cm^{-1}, probably arising from zirconia-modified methoxy species adsorbed on alumina, for the ZrO_2/Al_2O_3 sample (Fig. 1d) makes unreliable a comparative estimation, using the relative intensity proportions of bands of on-top methoxy species adsorbed on cerium or zirconium cations [7], of the surface composition of the $CeZrO_4$-containing samples.

Further information on the surface properties of these samples, at both a morphological and redox level, can be obtained by EPR using oxygen as probe molecule [10,13]. Fig. 2a–c show the EPR spectra observed after oxygen adsorption on the samples outgassed at 773 K. These are composed by different superoxide overlapping signals, whose characteristics and contributions to the spectra are displayed in Table 1.

Attribution of these signals is made on the basis of previous experience on ceria or Zr–Ce mixed oxide related materials [10,11,13–16]. Thus, the superoxide nature of (using formal charges) O_2^-–Ce^{4+} species is based on their similarity to signals of this kind observed in experiments of adsorption of ^{17}O-enriched oxygen mixtures [10,14]. The difference between signal OC′ and signals OC1,OC2, OC2′ or OC3 is related to the degree of coordinative unsaturation of the Ce cations where superoxides are stabilised, the former signal being formed on centres containing associated anionic vacancies [10]. This is based on differences in their EPR parameters along with the particular thermal preconditioning required for generation of each kind of defect [10], as well as on the specific activity for low-*T* NO reduction of centres giving rise to signal OC′ [16]; noteworthy, direct evidence on the presence of associated vacancies at ceria surfaces has been obtained by STM [17]. Apart from their different EPR

Table 1
Characteristics of the EPR signals observed after oxygen adsorption at RT on the samples outgassed at 773 K

Signal	EPR parameters[a]	Assignment	Intensity (μmol g^{-1}_{CeZrO4})[b]		
			10CZA	33CZA	CZ
OCA1 OCA2	$g_\perp$=2.025, $g_\parallel$=2.012 g_z=2.026, g_x=2.016, g_y=2.011	O_2^-–Ce^{4+} formed on 2D entities	4.8	2.0	–
OC′	g_z=2.042, g_y=2.010–2.009, g_x=2.009–2.008	O_2^-–Ce^{4+} formed on associated vacancies of aggregated CZ entities	–	–	0.7
OC1 OC2 OC2′ OC3	g_z=2.033, g_x=2.013, g_y=2.011 g_z=2.035, g_x=2.012, g_y=2.011 $g_\parallel$=2.034, $g_\perp$=2.011–2.010 g_z=2.031, g_x=2.017, g_y=2.011	O_2^-–Ce^{4+} formed on isolated vacancies of aggregated CZ entities	0.5	1.3	0.3
OZ OZ′	g_z=2.033, g_y=2.009, g_x=2.002 g_z=2.037, g_y=2.009, g_x=2.002	O_2^-–Zr^{4+}	0.4	0.5	0.8

[a] Axes attribution follows criteria of previous work [10].
[b] Evaluated by double integration of the spectra and comparison with a copper sulphate standard, and considering computer simulation results.

parameters, differences between signals type OCA (OCA1 and OCA2) and the other $O_2^- – Ce^{4+}$ signals concern mainly the fact that the former appear exclusively on alumina-supported samples [14,15]. Other differential aspects are the lower stability of signals type OCA towards outgassing at RT [14,15]. These facts reveal that superoxides type OCA are formed on highly dispersed cerium cations in direct interaction with the alumina surface. Recent work based on EPR, UV–vis and XANES indicates that the corresponding entities belong to two-dimensional patches (2D entities) dispersed on the alumina surface [15]. On the other hand, signals OZ and OZ′ are attributed to $O_2^- – Zr^{4+}$ species [13,18].

The presence of signals type OCA in 10CZA and 33CZA evidences that the mixed oxide forms 2D patches on these samples in addition to the 3D mixed oxide entities revealed by the bulk characterisation techniques. The nature of the 2D entities with regard to their composition is difficult to ascertain on the basis of these EPR experiments. However, previous work showing the absence of formation of $CeAlO_3$ in the X-ray diffractogram of these alumina-supported samples reduced under H_2 at 1173 K [11] suggests that 2D entities can present both Ce and Zr cations.

Further relevant details, not collected by Table 1, concern that, among $O_2^- – Zr^{4+}$ species, signal OZ is the only one observed for 10CZA and 33CZA while CZ presents exclusively signal OZ′. Additionally, signals OC1 and OC2 appear exclusively on 10CZA and 33CZA while CZ shows OC2′ and OC3 is common to the three samples. These differences, along with the absence of formation of associated vacancies in 10CZA and 33CZA (Table 1), are ascribed, in correlation with previous work on alumina-supported ceria samples [15], to the different characteristics of unsupported-$CeZrO_4$ in comparison to the small size 3D-$CeZrO_4$ particles present on the alumina-supported samples. This can be attributed to an epitaxial relationship between the mixed oxide and the alumina which affects the surface structural and redox properties of 3D-$CeZrO_4$ particles dispersed on alumina.

Significant differences are observed in the behaviour of the superoxide species when the samples are subjected to outgassing at RT. Thus, while no important changes are produced in the spectrum of sample CZ, for samples 10CZA and 33CZA (Fig. 2d and e), that treatment produces the disappearance of signals OCA1, OCA2 and OC2, which are recovered by subsequent oxygen adsorption. This suggests that OC2 might be related to positions within 3D-$CeZrO_4$ in contact with the alumina surface. The $O_2^- – Ce^{4+}/O_2^- – Zr^{4+}$ intensity ratio observed after this outgassing treatment (which is close to 1:1 in the three samples [11,13]), along with the relatively high intensity of $O_2^- – Zr^{4+}$ formed compared to pure zirconia [13], suggest that a mixed oxide type structure with composition close to the nominal ones is present at the surface of the $CeZrO_4$ particles.

Further experiments have been focussed to investigate the surface redox properties of the mixed oxide entities in 10CZA by heating in the closed cell after generation of superoxide species upon oxygen adsorption at RT (without RT outgassing), Fig. 3. The intensity losses in these experiments can be attributed to surface oxidation processes leading to generation of diamagnetic species [10]. The significantly larger stability of superoxides formed on 2D-entities in these experiments, their lower stability towards outgassing at room temperature (Fig. 2d,e) and the milder thermal preconditioning required for their formation [14] indicates the higher surface reducibility of 2D entities as well as the greater difficulty for their oxidation with respect to 3D-$CeZrO_4$ particles. The comparatively higher stability of OCA1 with respect to OCA2 (Fig. 3B) is related to their different location, respectively, at border and surface positions, within 2D entities [14,15].

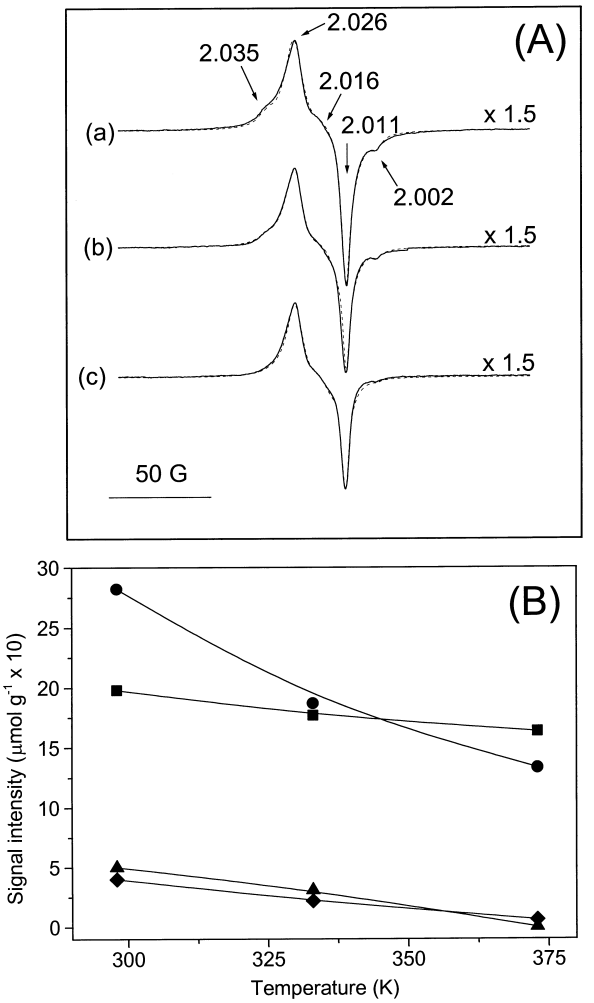

Fig. 3. (A) EPR spectra at 77 K of 10CZA. (a) After oxygen adsorption at RT on the sample outgassed at 773 K; subsequent heating in the closed cell at (b) 333 K and (c) 373 K. Computer simulations are overlapped as dashed lines. (B) Evolution of signals OCA2 (circles), OCA1 (squares), OC1–OC2 (triangles) and OZ (diamonds) in the course of the experiments of Fig. 3A.

4. Conclusions

Analysis of FTIR spectra of on-top methoxy species adsorbed on Ce or Zr cations suggest formation of Ce–Zr mixed oxide type structures at the surface of $CeZrO_4$ and alumina-supported $CeZrO_4$ samples although comparison with reference alumina and ZrO_2/Al_2O_3 materials points out the difficulty for estimating the surface composition from these spectra. EPR spectra of superoxide species, supplementing previous work on these samples [11,13], reveal the presence of 2D and 3D Zr–Ce mixed oxide entities on the alumina-supported samples, the former being more easily reducible and more difficult to oxidise than the latter. On the other hand, the different characteristics of superoxides present on unsupported $CeZrO_4$ and alumina-supported $CeZrO_4$ samples evidence the influence of alumina on the growing of 3D Zr–Ce mixed oxide particles.

Acknowledgements

A.M.-A. and A.B. H. thank the Comunidad de Madrid for grants under which this work was carried out. Financial support from CAICYT (Project no. MAT 97-0696-C02-01) and CAM (Project no. 06M/084/96) is acknowledged.

References

[1] R.J. Farrauto, R.M. Heck, Catal. Today 51 (1999) 351.
[2] J.P. Cuif, G. Blanchard, O. Touret, A. Seigneurin, M. Marczi, E. Quémere, SAE 970463, 1997.
[3] J. Kašpar, P. Fornasiero, M. Graziani, Catal. Today 50 (1999) 285.
[4] G. Vlaic, R. Di Monte, P. Fornasiero, E. Fonda, J. Kašpar, M. Graziani, J. Catal. 182 (1999) 378.
[5] G. Vlaic, P. Fornasiero, S. Geremia, J. Kašpar, M. Graziani, J. Catal. 168 (1997) 386.
[6] A. Martínez-Arias, M. Fernández-García, V. Ballesteros, L.N. Salamanca, J.C. Conesa, C. Otero, J. Soria, Langmuir 15 (1999) 4796.
[7] G. Colón, M. Pijolat, F. Valdivieso, H. Vidal, J. Kašpar, E. Finocchio, M. Daturi, C. Binet, J.C. Lavalley, R.T. Baker, S. Bernal, J. Chem. Soc. Faraday Trans. 94 (1998) 3717.
[8] E. Finocchio, M. Daturi, C. Binet, J.C. Lavalley, G. Blanchard, Catal. Today 52 (1999) 53.
[9] F. Fally, V. Perrichon, H. Vidal, J. Kašpar, G. Blanco, J.M. Pintado, S. Bernal, G. Colón, M. Daturi, J.C. Lavalley, Catal. Today 59 (2000) 373.
[10] J. Soria, A. Martínez-Arias, J.C. Conesa, J. Chem. Soc. Faraday Trans. 91 (1995) 1669.
[11] M. Fernández-García, A. Martínez-Arias, A. Iglesias-Juez, C. Belver, A.B. Hungría, J.C. Conesa, J. Soria, J. Catal. 194 (2000) 385.
[12] M.H. Yao, N.J. Blaird, F.W. Kunz, J. Catal. 166 (1997) 67.
[13] A. Martínez-Arias, M. Fernández-García, C. Belver, J.C. Conesa, J. Soria, Catal. Lett. 65 (2000) 197.
[14] J. Soria, J.M. Coronado, J.C. Conesa, J. Chem. Soc. Faraday Trans. 92 (1996) 1619.
[15] A. Martínez-Arias, M. Fernández-García, L.N. Salamanca, R.X. Valenzuela, J.C. Conesa, J. Soria, J. Phys. Chem. B 104 (2000) 4038.
[16] A. Martínez-Arias, J. Soria, J.C. Conesa, X.L. Seoane, A. Arcoya, R. Cataluña, J. Chem. Soc. Faraday Trans. 91 (1995) 1679.
[17] H. Nöremberg, G.A.D. Briggs, Phys. Rev. Lett. 79 (1997) 4222.
[18] M. Anpo, M. Che, B. Fubini, E. Garrone, E. Giamello, M.C. Paganini, Topics Catal. 8 (1999) 189.